AIAA AVIATION Forum
5-9 June 2017, Denver, Colorado
23rd AIAA/CEAS Aeroacoustics Conference

10.2514/6.2017-3868

The Ingestion of Wake Turbulence into an Open Rotor

Nicholas J Molinaro[1], N. Agastya Balantrapu[1], Christopher Hickling[1],
W. Nathan Alexander[2] and William J Devenport[3]
Center for Renewable Energy and Aerodynamic Technology, Virginia Tech, Blacksburg, VA, 24060

Stewart A. L. Glegg[4]
Florida Atlantic University, Boca Raton, FL, 33431

A study of the acoustics and aerodynamics of a rotor ingesting a planar two-dimensional turbulent wake of a circular cylinder is presented. Detailed turbulence measurements were made in the undisturbed wake including the full cross sectional space time correlation function of its turbulence. Sound measurements were made of the wake ingestion into the rotor for rotor advance ratios varying from zero to high thrust, for rotor yaw angles from -15 to 15 degrees, and for a range of wake strike positions on the rotor disk. Probes mounted on two of the rotor blades were used to measure upwash fluctuations seen in the rotating frame, as well as blade to blade coherence spectra. The relationship between the rotor sound spectrum, in particular the formation of "haystacks" due to multiple cutting of large eddies, and the different scales of the ingested turbulence is assessed. The sound directivity is determined by the direction of the blade normals where the rotor is cutting the most intense wake turbulence and variations in sound intensity seen with yaw angle and strike location can be explained in these terms. On blade measurements show significant distortion of the incoming wake at high thrust conditions.

I. Introduction

Rotor systems operating in non-uniform turbulent flow are not uncommon. Compressor and turbine blade systems in aircraft engines, marine propellers, and helicopter rotor systems may all ingest in-coming turbulence which could be from the atmosphere, boundary layers on a nearby flow surface or wakes from upstream blades. The interaction of the rotor blades with the turbulence generates noise due to unsteady loading on the blades. Generally, the turbulence is inhomogeneous and anisotropic which makes the job of understanding these interactions more difficult. Sevik [1] was among the first to study rotor turbulence ingestion. He performed experiments on a 10-blade propeller mounted in a water tunnel downstream of turbulence generating grids of varying size. Sevik measured the unsteady thrust force acting on the rotor. He assumed that the ingested turbulence was both homogeneous and isotropic. Sevik saw good agreement between his predictions and his measurements with the exception of humps or haystacks at multiples of the blade passage frequency. These haystacks arise when an eddy is cut multiple times by successive blades. This cutting of a coherent structure produces a correlated unsteady blade loading and therefore broadband sound at the blade passage frequency and its harmonics. Many authors have observed or studied this haystacking phenomenon , including Sharpf and Mueller [2], Minniti *et al.* [3, 4], Wojno *et al.* [5, 6], Ganz *et al.* [7] and Stephens and Morris [8], all of whom except Ganz *et al.* used Sevik's rotor geometry.

The particular focus of this project is to study the ingestion of planar turbulent shear flows with the goals of providing the data and understanding needed for the development of both low order analytical models and the validation of high-fidelity computational simulations. This work is applicable to both marine and air vehicles. Many UAVs and marine vessels use rear mounted propellers. Surface discontinuities and appendages produce wakes that convect downstream and may eventually be drawn in by a rotor. Rotors are often mounted so as to ingest the vehicle

---

[1] Graduate Research Assistant, Department of Aerospace and Ocean Engineering, AIAA Student Member.
[2] Assistant Professor, Department of Aerospace and Ocean Engineering, AIAA Member.
[3] Professor, Department of Aerospace and Ocean Engineering, AIAA Associate Fellow.
[4] Professor, Department of Ocean and Mechanical Engineering, AIAA Associate Fellow.

boundary layer. A non-uniform turbulent flow impacting a rotor can be an extremely complicated problem. Just the documentation of the inflow boundary condition can pose a formidable challenge. However, many of these complexities reflect application specific details that do not change the fundamental physics of the interaction and sound generation. Our approach in this study is to examine the aerodynamics and acoustics of a simple straight bladed rotor ingesting two-dimensional turbulent shear flows – flows that are both inhomogeneous and anisotropic but that are dimensionally simple enough to permit complete documentation of the excitation they provide to the rotor, at least in the linear sense.

The first flow studied was the ingestion of a thick equilibrium turbulent boundary layer. Morton *et al.* [9] documented the complete cross-sectional space-time correlation of this flow to serve as the inflow boundary condition Alexander *et al.* [10], Wisda *et al.* [11, 12] and Murray *et al.* [13] examined the rotor sound field and Alexander *et al.*[14] studied this flow in terms of direct measurements of the blade-to-blade upwash correlations experienced on the rotor. Glegg *et al.* [15, 16] made predictions of the rotor noise based on the measured inflow correlations. The broadband haystacked spectra were found to be predictable for low and moderate thrust cases – the haystacking intensifying with thrust due to stretching and elongation of the eddies drawn into the rotor face. At high thrust, however, experiments showed the haystack peaks becoming almost tonal, at odds with linear predictions, because of local separation of the boundary layer around the blade tips. Murray [17] documented the structure of resulting highly unsteady flow, known as a propeller-hull vortex, and Glegg *et al.* [18] showed that the sharp spectral peaks could be explained by blade vortex interactions with the components of this structure. This case has been adopted as fundamental test case three (FC3) of the AIAA Fan Broadband Noise Prediction Workshop (http://web1.oai.org/FBNWorkshop.nsf/Index).

This paper is concerned with describing experimental results from the second flow studied – the ingestion of a planar turbulent wake shed by a circular cylinder. The first acoustic results from this study were presented by Alexander *et al.* [19]. In this paper we fill out much of this study, complementing further discussion of the acoustic field generated by the rotor with new measurements documenting the complete 4-dimensional correlation of the undisturbed wake used as inflow, as well as upwash velocity and blade-to-blade upwash correlation measurements made in the rotating frame. Where appropriate, results are compared with those from the boundary layer ingestion work showing substantial differences in behavior due to the different structure, extent, intensity and behavior of these flows. A second part of this study, involving the use of advanced beamforming strategies to reveal the distribution of acoustic sources over the rotor face, is presented by Hickling *et al.* [20]. Glegg *et al.* [21] have presented a parallel study involving analytically based predictions of the rotor noise. Large eddy simulations of the rotor wake interaction are presented by Wang *et al.* [22].

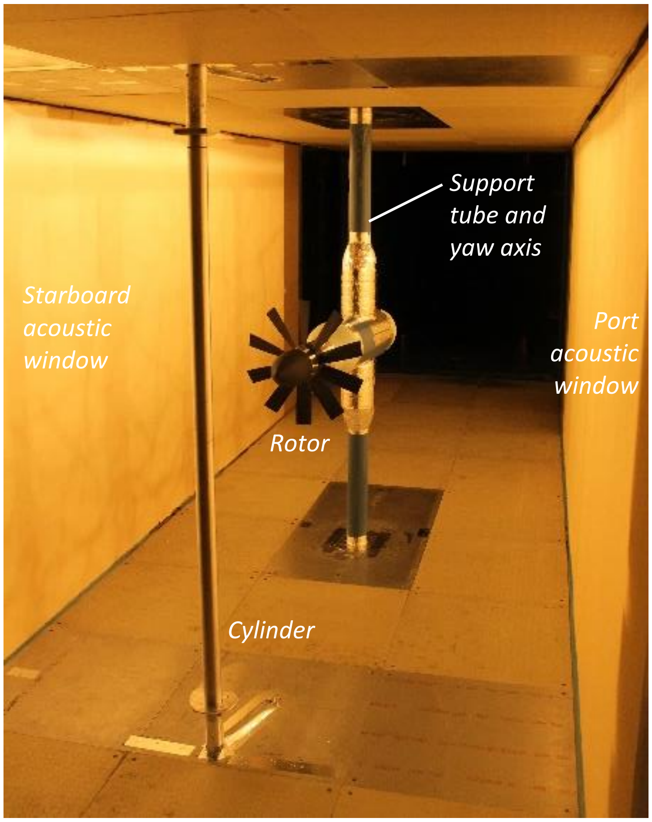

Figure 1. Cylinder and rotor mounted in the anechoic test section of the Virginia Tech Stability Tunnel.

II. Apparatus and Instrumentation

A. Stability Wind Tunnel

Measurements were performed in the hybrid anechoic test section of the Virginia Tech Stability Wind Tunnel. 4.2-m long tensioned Kevlar acoustic windows form the two side walls of the 1.85 by 1.85-m square test section. Sound generated in the test section flow radiates through these into anechoic chambers where microphones are placed. At the same-time the windows keep the flow contained within the test section, minimizing aerodynamic interference effects. The test section floor and ceiling are formed by Kevlar flow surfaces backed by acoustic absorbers. The facility is anechoic down to 180Hz. Flow in the empty test section is closely uniform and of very low turbulence level (0.021% at 21m/s). Further facility details are given by Devenport *et al.* [23].

B. Rotor

The rotor used in this study is a left-handed 2.25:1 scale model of that first used by Sevik [1] and has a diameter of 457 mm with a 127 mm hub, Figures 1 and 2. The hub is slightly over size, absorbing 6.4-mm of each blade root in order to accommodate rotating-frame instrumentation. The rotor has 10 square tipped blades each with a chord of

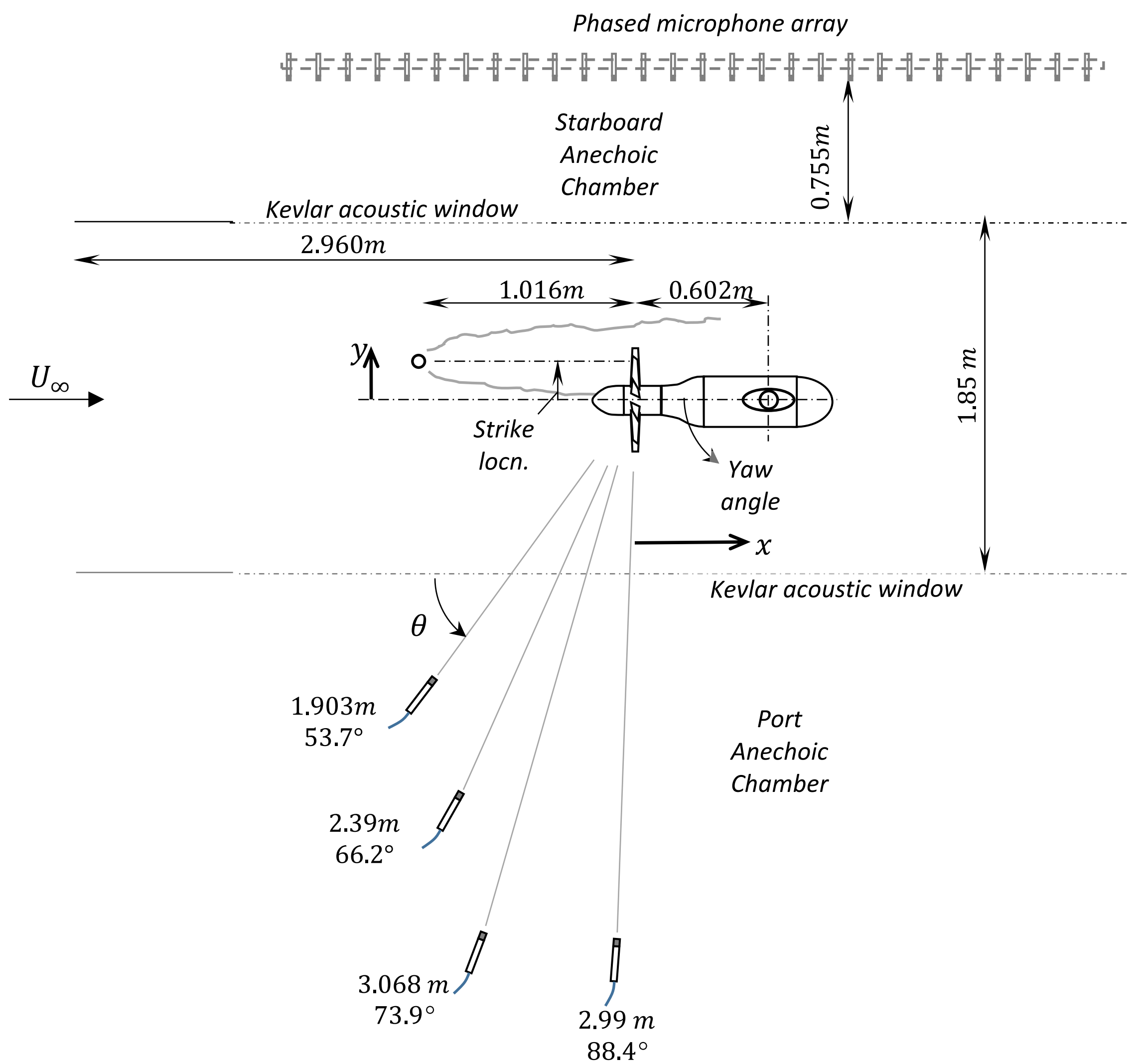

Figure 2. Plan view schematic of the anechoic test section showing the rotor and cylinder locations, microphone instrumentation locations, and definition of the coordinate system. Single microphone locations given in observer angle θ and radius to the unyawed rotor disk center.

57.2 mm. The blades are twisted from a pitch angle of 55.6 degrees at the hub to 21.2 degrees at the tips and have a thickness to chord ratio close to 9%. The design advance ratio is 1.17 and the zero-thrust advance ratio is 1.44 estimated using JavaProp [11]. The rotor is powered by an AKM-64P-ACCNDA00 Kollmorgen servomotor at speeds of up to 4500 rpm. The motor is contained within a 219-mm diameter fairing downstream of the rotor, the upstream end of which is 306 mm downstream of the rotor disk plane. The two are connected by a section of 127-mm diameter hub, covered by a foam fairing at the downstream end that gradually increases the diameter to 219 mm. The 127-mm diameter rotor nose cone extends 216-mm forward of the blade leading edge plane. The rotor assembly is mounted from an 88.9-mm diameter vertical tube located towards the downstream end of the motor housing. Approximately 300-mm long sections of the tube, immediately above and below the motor housing are contained within streamwise-oriented airfoil section fairings. The tube connects the rotor assembly to the tunnel structure and the yaw traverse, embedded in the test section ceiling. The tube is centered in the test section 3.56m aft of the test section entrance and defines the yaw axis, Figure 2. At zero yaw the center of the rotor disk is 602-mm upstream of this axis. Coordinates are defined relative to the center of the rotor disk at zero yaw, with x measured downstream, y laterally, toward the starboard side, and z spanwise (and upwards) so as to complete a right handed system. The rotor turns clockwise as seen looking downstream.

C. Cylinder Model

A 50.8 mm diameter cylinder, mounted vertically in the test section, was used to generate the wake. The cylinder was mounted 20 diameters D upstream of the rotor disk at zero yaw, a distance of 1016-mm. The cylinder mounting allowed for its lateral y position to be adjusted to vary the strike location of the wake center on the rotor. Strike locations are referred to in terms of rotor radius R. Thus a strike at 100% starboard implies that the cylinder was placed with its axis at the same y location as the starboard-side edge of the rotor disk. At 0% the wake strikes the center of the disk. When the rotor yaw angle was changed the lateral position of the cylinder was adjusted to maintain the same strike location on the rotor disk. Fences were placed on the cylinder 165-mm from the floor and ceiling to improve the two-dimensionality of its wake, verified using cross sectional measurements with the rotor system removed [19].

D. Hotwire Systems

D.1 Constant Temperature Anemometry Measurements

Hotwire probes were used to measure the cylinder wake characteristics in the absence of the rotor. Most measurements were made using 4-sensor probes, known as quad wire probes. Probes were manufactured by Auspex Corporation (type AVOP-4-100). The probes consist of two orthogonal X-arrays and are able to measure 3 components of velocity from within a measurement volume of 0.75 mm^3. Wittmer *et al.* [24] describe the design, calibration, and validation of the probes. Probes were calibrated for flow angle and velocity, and measurements were corrected for temperature drift using the method of Bearman [25].

Measurements were made in two phases. In the first phase, 3-component profiles of mean velocity, turbulence stresses and velocity spectra were measured through the cylinder wake at the mid-height ($z = 0$) of the Stability Tunnel test section. The measurements at a free stream velocity of 20m/s, corresponding to a cylinder diameter Reynolds number of 59,000±2000, were made at $(x - x_{cyl})/D = 10$, 15 and 20, this last station representing the undisturbed wake structure at the rotor location.

Measurements in the second phase were conducted in the 0.71 by 0.71-m square test section of the Virginia Tech Open Circuit wind tunnel. This facility has a settling chamber with screens and a honeycomb, a 5.5:1 contraction and a 1.22-m long test section in which the free stream turbulence levels are close to 0.5%. Measurements were performed at a free stream velocity of 26 m/s and with a 38.1-mm diameter cylinder model, resulting in the same cylinder Reynolds number and thus equivalent flows. Measurements were made at $(x - x_{cyl})/D$ = 20. This auxiliary facility was used because it was better suited to the time consuming task of documenting the full 4-dimensional space-time correlation function of the cylinder wake. In general, the two-point space time correlation function of a statistically stationary flow is an 7-dimensional function of two spatial coordinates $\boldsymbol{r} = (x, y, z)$ and $\boldsymbol{r}' = (x', y', z')$, and time delay τ. However, if we restrict ourselves to the cross-sectional plane (inferring streamwise correlations when needed using Taylor's hypothesis) and use the homogeneity of the two-dimensional wake in the spanwise direction then this reduces to 4 dimensions, specifically $R_{ij}(y, y', \Delta z, \tau) = E[u_i'(y, z, t)u_j'(y', z + \Delta z, t + \tau)]$ where $E[\,]$ denotes expected value. Note that we use both (u, v, w) and (u_1, u_2, u_3) to denote velocity components in the (x, y, z) directions, respectively. Measurement of this function therefore requires two three-component hot-wire probes to measure the time delay correlation tensor between every point in the wake profile and every other for a comprehensive set of spanwise separations. This is a process that has to be optimized, but still required measurement of some 2500 point pairs as well as extensive post processing to condense the data to a tractable form. See Molinaro [26] for details.

D.2 Constant Voltage Anemometry Measurements

Measurements of the instantaneous upwash velocities experienced at the blade tips were made using cross-wire probes attached to two specially constructed rotor blades, Figure 3. This is the same system that was employed by Alexander *et al.* [14] in their boundary layer ingestion studies. Six total cross wire probes were bonded to the pressure side of two successive rotor blades. The measurement volumes of the probes were positioned 19 mm upstream of the blade leading edges. This spacing was chosen such that the blade did not influence the probe sensors and was determined using potential flow theory. The probes were operated using a custom 4 channel constant voltage anemometer designed by Tao Systems mounted inside the rotor nose cone and spun with the rotor blades. The hotwire signals were transmitted to the non-rotating frame using a Moog Model AC6231 slip ring, limited to rotational speeds of 2500 rpm and below. Measurements were taken using an NI 9220 cDAQ system sampled at 51.2 kHz for 30 seconds. A sawtooth signal from the motor controller was recorded simultaneously with the hotwire signal so that the absolute positions of the blades could be determined. Data from two of the probes is presented in this paper (other probes did not survive to generate useful data) these being at 95%R on the leading blade and 90%R on the trailing blade. Note that uninstrumented blades were used for all acoustic measurements.

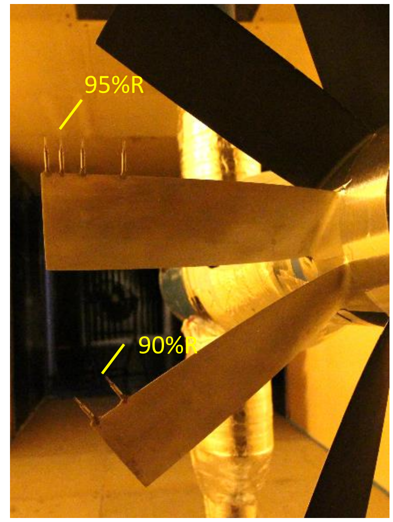

Figure 3. View from upstream of the instrumented rotor blades showing the two probes for which results are reported

E. Microphone Setup

Acoustic results presented in this paper were either measured using single microphones or a microphone phased array. The 251 channel phased array was setup in the anechoic chamber on the starboard side of the test section, Figure 2. The array features four interwoven spirals each made up of about 62 microphones (see Figure 4 of Alexander *et al.*[19]). Each individual microphone is also of high enough quality to provide valid acoustic data. The maximum microphone separation is 3.82 m while the minimum spacing is 30 mm. Each microphone is a G.R.A.S Type 40PH-S5 free field array microphone with a frequency range of 10 Hz to 20 kHz and a dynamic range of 32 dB to 135 dB. The phased array and the associated acquisition and reprocessing software was built for the Stability Tunnel by AVEC Inc. Microphone signals were sampled at 51.2kHz.

The four single ½ inch B&K microphones were set up in the anechoic chamber on the port side of the test section in the $y - z$ plane, at the receiving angles and distances indicated in Figure 2. The microphone acquisition was handled by a 3050-A-060 LAN-XI DAQ which provided 24-bit resolution and a sampling rate of 65.5 kHz.

A second configuration of microphones, including a split array placed on both sides of the test section, was used for some experiments. Results from those measurements are presented by Hickling *et al.* [20].

F. Stability Tunnel Test Matrix

The acoustic test matrix consisted of 325 run conditions with different combinations of rotor advance ratios and yaw angles, and strike locations of the wake on the rotor disk. All measurements were made for a fixed free stream velocity U_∞ of 20±0.1 m/s corresponding to a Mach number of 0.057 and cylinder Reynolds number of 59,000. A total of 13 advance ratios, distributed from zero thrust $J = 1.44$ to high thrust $J = 0.58$, were studied at each of five yaw angles $(-15°, -7.5°, 0, 7.5°, 15°)$ and five wake/rotor strike locations port side (100%R and 75%R, center strike (0%), starboard side 75%R and 100%R).

The on-blade hotwire text matrix included measurements with the rotor unyawed and with the wake striking at the center of the rotor and 75%R to port. Again a detailed set of advance ratios was considered including 18 values between J =1.44 and 0.58. Because of limitations on the slip ring RPM not all measurements could be made at a 20m/s free stream velocity. Measurements at advance ratios below 1.05 were made by reducing the free stream velocity to 15±0.1 m/s, and below 0.78 by reducing it to 10±0.1 m/s. These measurements assume reduction in the cylinder Reynolds numbers to 45,000 and 30,000 did not significantly alter the non-dimensional form of its turbulence structure.

III. Results and Discussion

A. Characteristics of the Undistorted Wake

Figure 4 shows mean velocity and turbulence stress profiles through the undisturbed wake measured in the Stability Tunnel at $(x - x_{cyl})/D$ = 20. Wake profiles have been centered by subtracting the wake center location designated as y_o. The wake is almost symmetric with a maximum mean velocity deficit, Figure 4(a), of 20% and an overall width of approximately 2 rotor radii R just sufficient to immerse almost the entire rotor face when the projected centerline of the wake is on the rotor axis. The turbulence normal stress profiles (Figure 4(b)) show levels to be quite high in the center of the wake with a peak intensity of about 14% in the v component. The anisotropy is evident here with normal-to-wake stress having the largest magnitude followed by the streamwise and spanwise stresses. The streamwise normal-stress profile is somewhat misleading as it includes contributions from some very low frequency

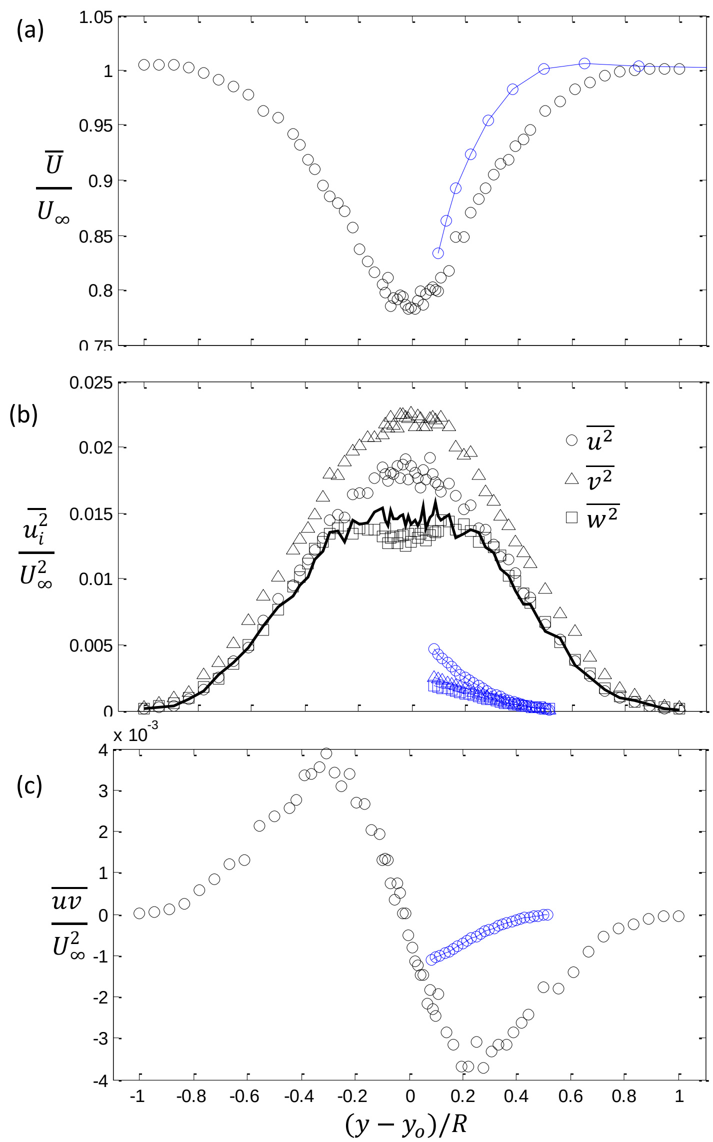

Figure 4. Velocity profiles through the cylinder wake at $(x - x_{cyl})/D$ = 20 (black markers) compared rotor-location boundary layer profiles from Morton *et al.* (2012) (blue markers). (a) Mean velocity profile, (b) Reynolds normal stresses (solid black line shows $\overline{u^2}/U_\infty^2$ after high pass filtering at $fD/U_\infty = 0.015$), (c) Reynolds shear stress profile. Distances normalized on the rotor radius R.

fluctuations. High-pass filtering at frequencies $fD/U_\infty > 0.015$ reduces levels to the profile indicated by the solid line, while having little discernable influence on the other stress components. We suspect that this is due to low-frequency flapping of the wake. Upwash measurements made in the rotor frame of reference, to be shown later, suggest that this motion may be stabilized when the rotor is installed. The Reynolds shear stress profile (Figure 4(c)) appears closely antisymmetric, with a peak magnitude of about $0.004U_\infty^2$.

Figure 5 shows correlation results for the wake, measured both in the Stability Tunnel and the auxiliary facility at $(x - x_{cyl})/D$ = 20. Figure 5(a) shows streamwise integral lengthscales inferred from integral timescales and Taylor's hypothesis. The u component fluctuations have the longest streamwise scale of between 20 and 30%R

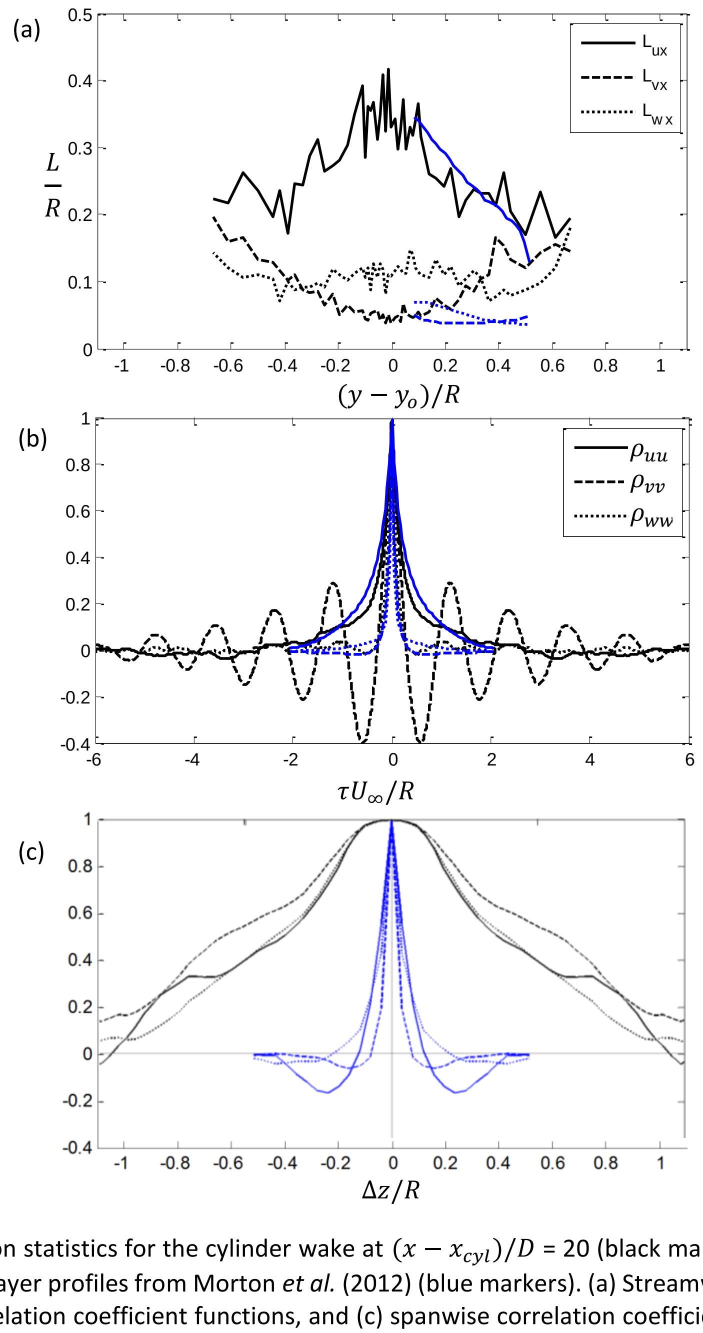

Figure 5. Correlation statistics for the cylinder wake at $(x - x_{cyl})/D$ = 20 (black markers) compared to rotor-location boundary layer profiles from Morton *et al.* (2012) (blue markers). (a) Streamwise integral scale profile. (b) Time delay correlation coefficient functions, and (c) spanwise correlation coefficient functions at the wake center and 20% of the boundary layer thickness. Legend for part (c) is same as part (b).

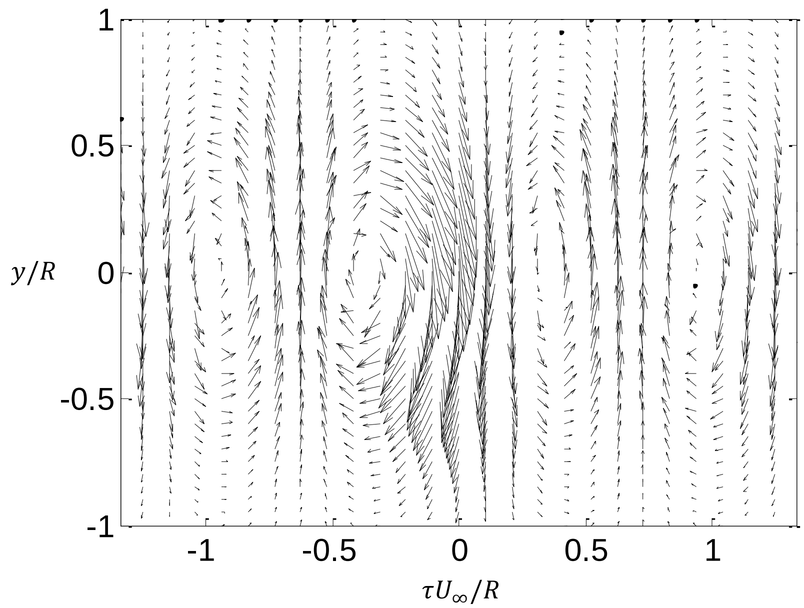

Figure 6. Dominant compact eddy structure for the cylinder wake at $(x - x_{cyl})/D$ = 20.

depending on position in the wake, whereas the integral scales of v and w are about half as large. Looking at the time delay correlation coefficient functions on the wake centerline, Figure 5(b), we see that v correlation function is oscillatory with a period close to $1.18R/U_\infty$ implying a Strouhal number, normalized on the cylinder diameter, fD/U_∞ of 0.19. This is therefore the coherent vortex shedding from the cylinder, and the streamwise integral scale in v is clearly much smaller than the true correlation distance because of the negative excursions in its correlation function. The u and w correlation functions have a much more monotonic form and decay to coefficients of 10% over timescales equivalent to streamwise distances of 90% and 20% of the rotor radius respectively. The spanwise correlation coefficient functions measured at the wake center, Figure 5(c) show more uniform behavior amongst the three velocity components, with correlation coefficients falling monotonically to 10% over about one rotor radius in all cases.

The full form of the two-point correlation wake data set is discussed by Molinaro [26]. The data set allows for the space time correlation in any frame of reference on any cut through the cross section to be inferred. It also permits statistical analysis of the typical eddy structures that populate the wake. Compact eddy structures [27] are one way of visualizing such eddies. The proper orthogonal decomposition of the wake is taken in the inhomogeneous y direction, and then the remainder of the correlation function is used to obtain the best linear stochastic estimate of the 3-dimensional velocity field associated with each mode. Specifically, the vector modal velocity profiles $\phi_i^{(n)}(y)$, and their associated eigenvalues $\lambda^{(n)}$, are obtained by solving the integral equation,

$$\int R_{ij}(y, y', 0,0)\phi_j^{(n)}(y')dy' = \lambda^{(n)}\phi_i^{(n)}(y)$$

The velocity field of the compact eddy structure associated with the nth mode is then,

$$u_j^{(n)}(y, \Delta z, \tau) = \frac{1}{\lambda^{(n)}}\int R_{ij}(y, y', \Delta z, \tau)\phi_j^{(n)}(y')dy'$$

Figure 6 shows a $y - \tau$ cross section through the compact eddy structure associated with the dominant proper orthogonal mode responsible for just over half the total turbulence kinetic energy in the wake. This visualization clearly shows the turbulent motions to be dominated by a coherent street of spanwise oriented alternating sign eddies.

B. Far-field sound generated by the rotor

Figure 7(a) shows contours of sound pressure level (SPL) referenced at $20\mu Pa$ as a function of the advance ratio at receiver angle θ of 53°, (Figure 2). These results are for the 100% starboard strike case where the cylinder axis

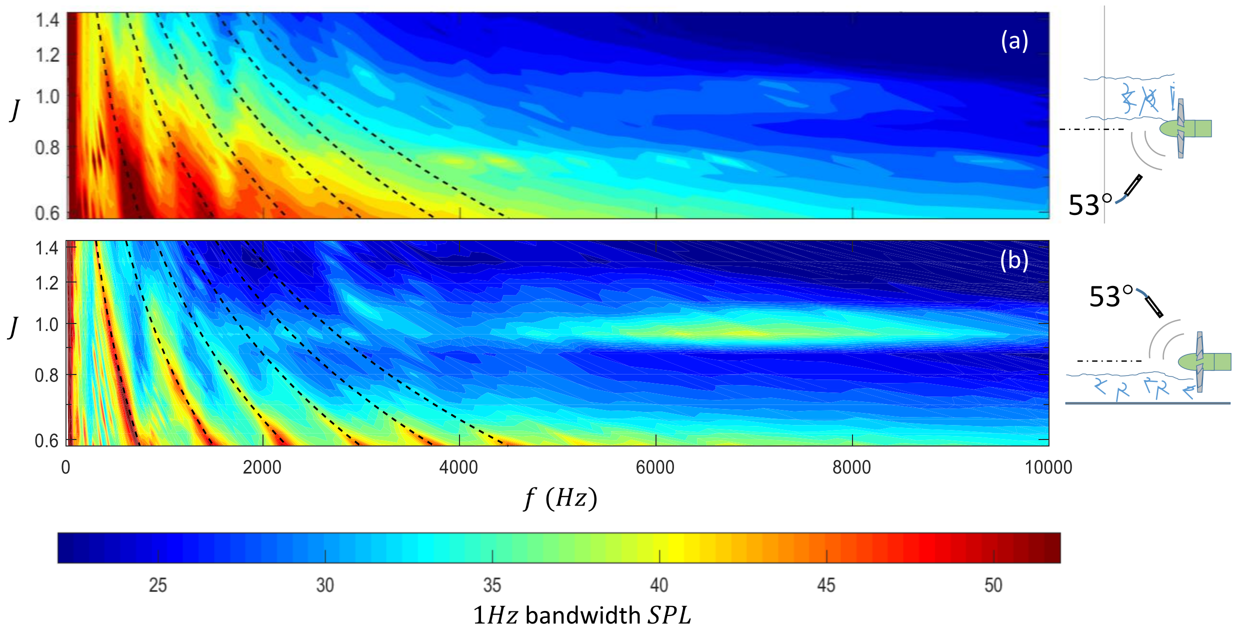

Figure 7. Far-field noise spectra at an observer angle of 53° plotted as a function of advance ratio for the unyawed rotor. Dashed lines show the blade passing frequency and harmonics. (a) Wake ingestion, 100% starboard strike. (b) Boundary layer ingestion (Wisda *et al.*, 2015), with the rotor immersed in the top 80% of the boundary layer thickness δ, $\delta/R = 44\%$. Spectral levels scaled to an observer distance of 1.903 m.

is at the same y location as the starboard edge of the rotor and about half the rotor face was immersed in the wake. The dashed lines denote the blade passing frequency (BPF) and its harmonics. The far-field sound is characterized by broad haystacks centered around the blade passing frequency and its multiples due to the unsteady coherent loading on successive blades of the rotor. Haystacking is first seen, at the blade passage frequency, at an advance ratio of about 1.3 and becomes more pronounced as the advance ratio is reduced, with a first harmonic appearing about $J = 0.95$ and a second harmonic at $J = 0.8$. Overall sound levels increase as the advance ratio is reduced because of the increase in rotor speed. The haystacking becomes more pronounced for the same reason – higher blade speed means a greater correlation between cuts of successive blades through the same turbulent eddy. The horizontal ridge visible at frequencies of above 5 kHz for advance ratios around 1 is believed to be the result of trailing edge noise produced by coherent vortex shedding from the rotor blades, similar to that observed by Wisda *et al.* [11] and Hersh *et al.* [28].

For comparison Figure 7(b) shows sound measurements of turbulent boundary layer ingestion into the same rotor from the study of Wisda *et al.* [12]. The rotor is again un-yawed, the free stream velocity is 20 m/s and the observer angle is 53°. Spectral levels have been scaled to reflect the the same observer radial distance (1.903 m, Figure 2) as the wake measurement. As shown in the thumbnail sketch in Figure 7(b) the outer 1/3rd of the rotor radius is immersed in the boundary layer. Overall, sound levels caused by the boundary layer ingestion are substantially lower than those produced by the wake. There are two reasons for this; the boundary layer covers a significantly smaller portion of the rotor disk, and it is much less turbulent than the wake. Figure 4 compares mean velocity and turbulence profiles measured over the portion of the boundary layer swept by the rotor (in blue), with those measured in the wake. Despite having a higher mean velocity gradient, turbulence stresses in the boundary layer are 1/3rd to 1/6th of those in the wake, and thus upwash fluctuations experienced by the blades will be proportionately smaller. There are also detail differences between the wake and boundary layer ingestion. The sound spectrum for the boundary layer shows a much stronger trailing edge noise signature (likely due to the much larger area of the rotor not exposed to turbulent inflow) and shows narrower more distinct haystacks that extend to higher harmonics at a given advance ratio. One reason for this is the large difference in the correlation scales between these two flows. Looking at the streamwise velocity component, which is the dominant contributor to the blade upwash, we see that this correlates over a somewhat larger streamwise extent in the boundary layer than in the wake (Figure 5(b)), but over a much smaller spanwise extent

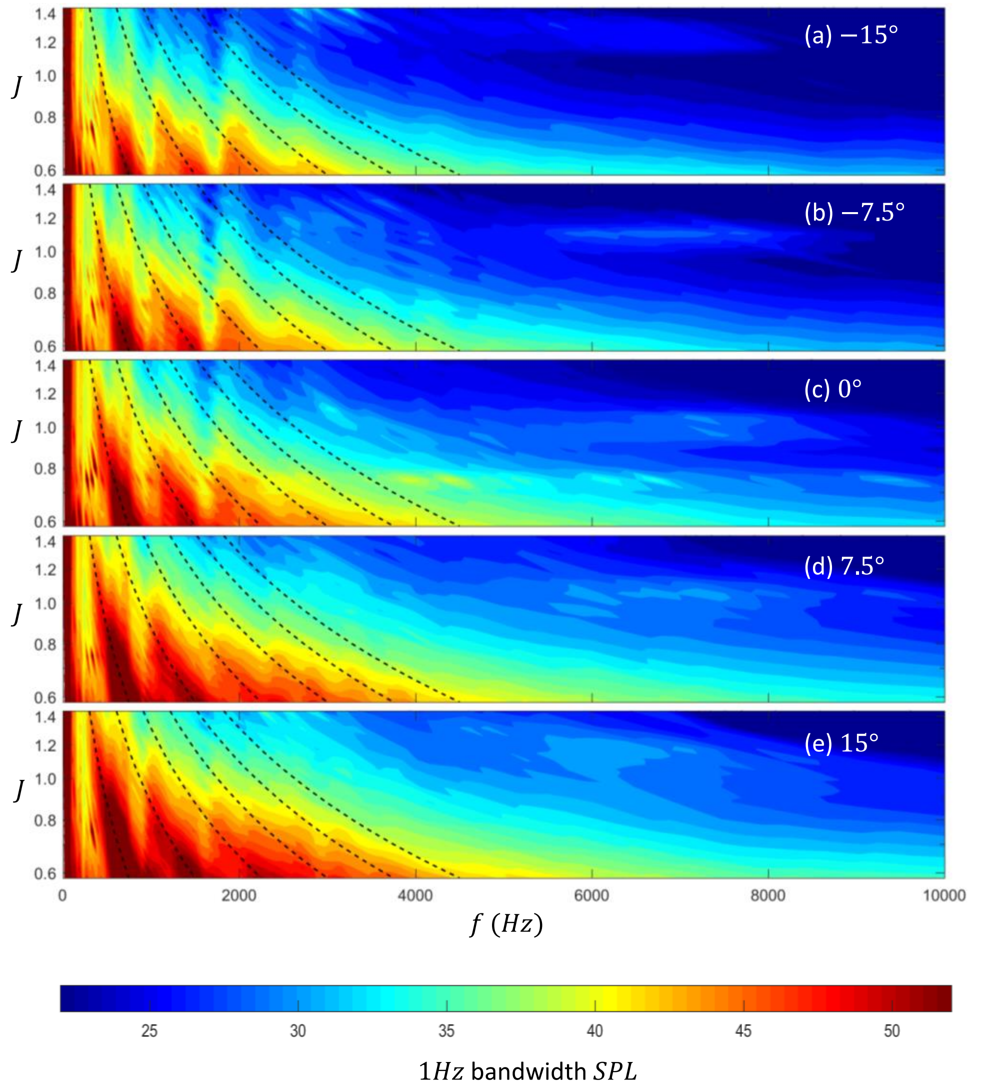

Figure 8. Far-field noise spectra at an observer angle of 53° plotted as a function of advance ratio for for different rotor yaw angles, 100% starboard strike. Dashed lines show the blade passing frequency and harmonics.

(Figure 5(c)). The successive blade interactions with the large eddies are therefore much more impulsive with the boundary layer (leading to higher harmonic content in the sound field) and tend to correlate for longer (leading to narrower haystacks). This effect is enhanced due to the presence of the rotor next to the wall when immersed in the turbulent boundary layer. The image of the rotor in the wall doubles the stretching of the turbulence as it is drawn into the rotor disk which organizes the eddies again making the interactions more impulsive and increasing the number of times which each eddy is cut. Note that, at very low advance ratios, the turbulent layer separates from the wall generating tone noise as the blades cut the separation eddies at the harmonics of the blade passing frequency – a mechanism that does not exist for the wake

Figure 8 shows the effects of rotor yaw on the sound generated by wake ingestion. The spectral map of Figure 7(a) is compared with similar maps recorded from the $\theta = 53°$ observer angle with the rotor at -15, -7.5, 7.5 and 15 degrees yaw. Figure 9 shows the same results for an observer angle of 74 degrees. This figure includes plots (to the right) showing the variation of OASPL with advance ratio for both 53° (in black) and 74° (in blue), obtained by integrating over the frequency range from half the BPF to 20 times the BPF, capturing the full range of the broadband noise while eliminating contamination at very low frequencies. As the rotor is yawed positively (Figures 8(c) through (e), overall spectral levels increase and the haystacks become less distinct. Negative yaw (Figures 8(a) through (c))

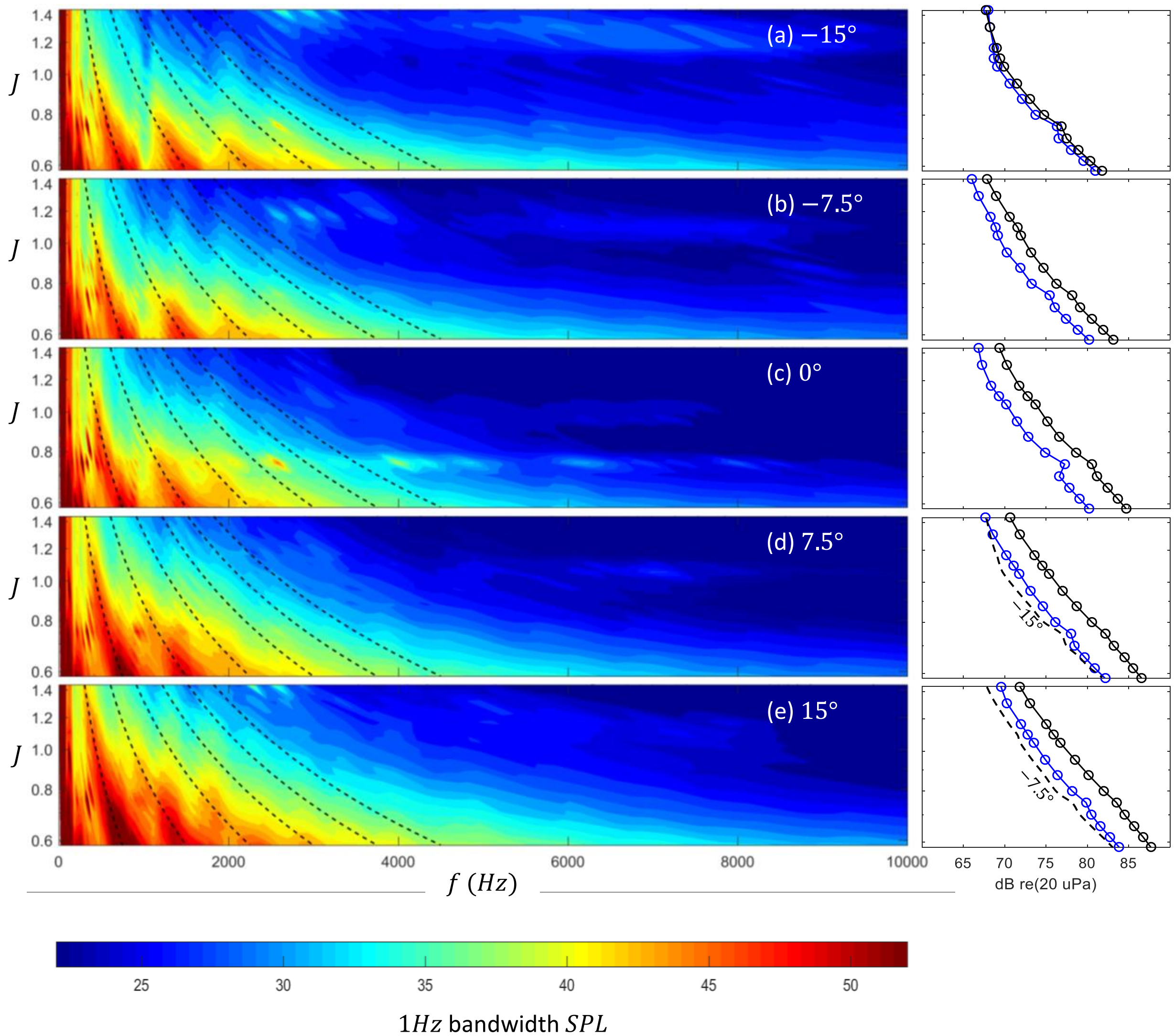

Figure 9. Far-field noise spectra at an observer angle of 74° plotted as a function of advance ratio for for different rotor yaw angles, 100% starboard strike. Dashed lines show the blade passing frequency and harmonics. Plots to the right of each contour set show OASPL as a function of advance ratio for observer angles of 53° (black) and 74° (blue) and use the same vertical axis as the spectral plots. Spectral levels scaled to an observer distance of 1.903 m.

produces the reverse effect. OASPL increases by about 6dB from -15 to 15 degrees yaw. Similar behaviors are seen at the 74-degree observer angle (Figure 9). The change in the degree of haystacking is likely due to the influence of yaw on the path taken by the rotor blades through the space time correlation of the wake. The noise results suggest that there is a reduction of the blade to blade correlation with positive yaw. The overall change in sound levels can be explained in terms of directivity. If we envision the sound field as turning with the rotor then a -15 to 15 degree change in yaw angle changes the angle of a fixed observer measured from the rotor axis by the same amount. Assuming the rotor sound field to be directed primarily along the rotor axis this results in an increase in sound levels with yaw. This equivalence between yaw and directivity holds quantitatively also. For example, an observer at $\theta = 53°$ is at an angle of 68° and 60.5° to the rotor axis for yaw angles of -15 and -7.5 degrees, almost the same angles seen at $\theta = 74°$ for yaw angles of 7.5° and 15° and thus sees similar sound levels. This is shown in the OASPL plots of Figures 9 (d) and

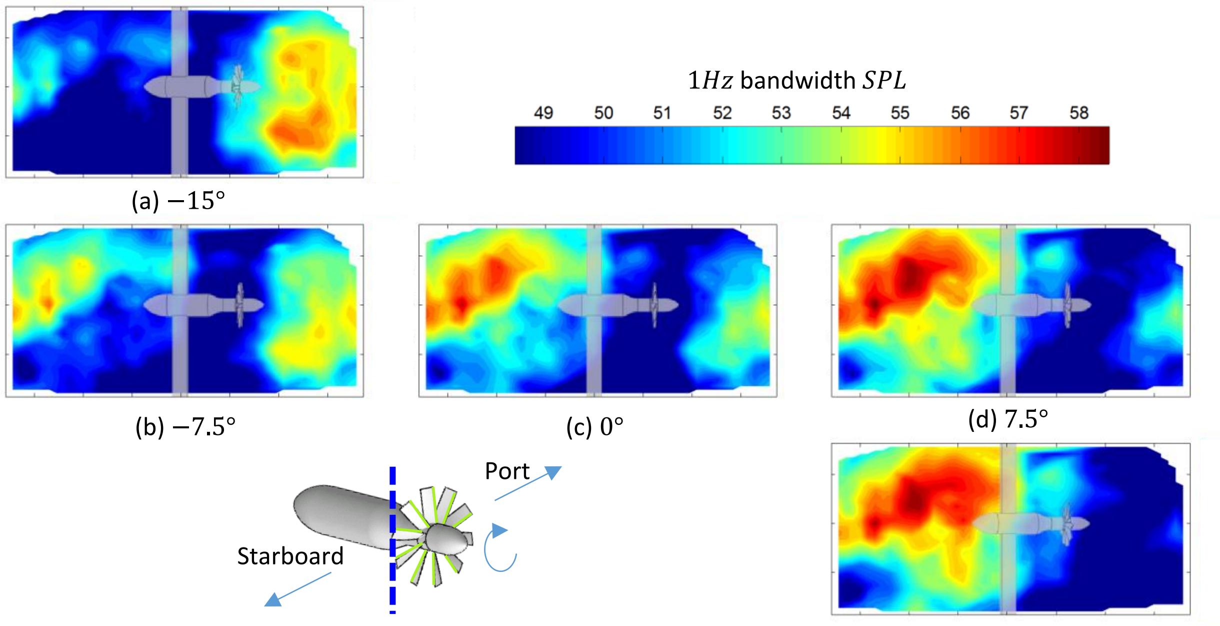

Figure 10. Contours of sound levels at 1BPF (547 Hz) measured on the starboard side of the rotor at an advance ratio J of 0.8 and 100% starboard strike location in a plane at y =1.68-m using the phased array, as a function of rotor yaw angle. Divisions on vertical and horizontal axis are at intervals of 0.5 m.

(e) where OASPLs measured at a receiver angle of 74° for yaw angles of 7.5° and 15° (blue curves) are compared with those measured at a receiver angle of 53° for yaw angles of -15 and -7.5 degrees (black dashed lines). Sound levels are the same, to within 1 to 2dB.

A more global view of the directivity of the sound field can be realized by looking at the phased microphone array results. Directivity maps at 1 BPF and an advance ratio J = 0.8 (moderate thrust) for the 100% starboard strike location of the wake for all yaw angles are presented in Figure 10. Directivity is shown here in terms of $x - z$ microphone position in the array relative to the rotor and mount location Each map represents 92 degrees of arc in the horizontal plane and 53 degrees in the vertical. Figure 10(c), corresponding to the unyawed case, shows the sound field appears to have a dipole-like directivity pattern with lobes forward and aft of the rotor and a null near the plane of the rotor disk. The dipole is not aligned with the rotor axis, but tilted down and to the right which can be understood by looking at blade orientations shown in the thumbnail sketch on the bottom left of Figure 10. The blue dashed line shows the strike location of the wake center and it can be seen that the blades immersed in the wake are facing downwards resulting in a downward facing dipole. Angling the rotor to negative yaw (Figures 10(a) and (b) directs the forward lobe of the dipole more onto the right hand side of the array, whereas positive yaw (Figures 10(d) and (e)) exposes the left-hand side of the array more to the rearward lobe. These directivity patterns are consistent with the acoustic non-compactness of the rotor, but the compactness of the blade chord, and can be usefully modeled using blade-normal oriented dipoles distributed along the line of intersection between the wake center plane and the rotor disk [19].

This overall directivity pattern is not just observed for the 100% starboard strike position but for all other strike positions. However, the orientation of the sound field depends on the blade orientations that are immersed in the wake. Figures 11 and 12 show the directivity maps for the centerline strike and 100% port side wake strike conditions, respectively. For the centerline strike case (Figure 11), the dipole pattern rotates as the rotor is yawed but is no longer noticeably tilted. Looking at thumbnail sketch for this case we see that where the rotor blades cross the center of the wake on the top of the disk the blade normals are directed towards the starboard side. On the bottom of the disk they are oriented towards the port side. As we move to the 100% port side wake strike location (Figure 12), the dipole-like pattern develops a tilt upward and to the right. This is because the rotor blade normals are tilted upwards on the port side of the rotor disk, where they pass through the center of the ingested wake.

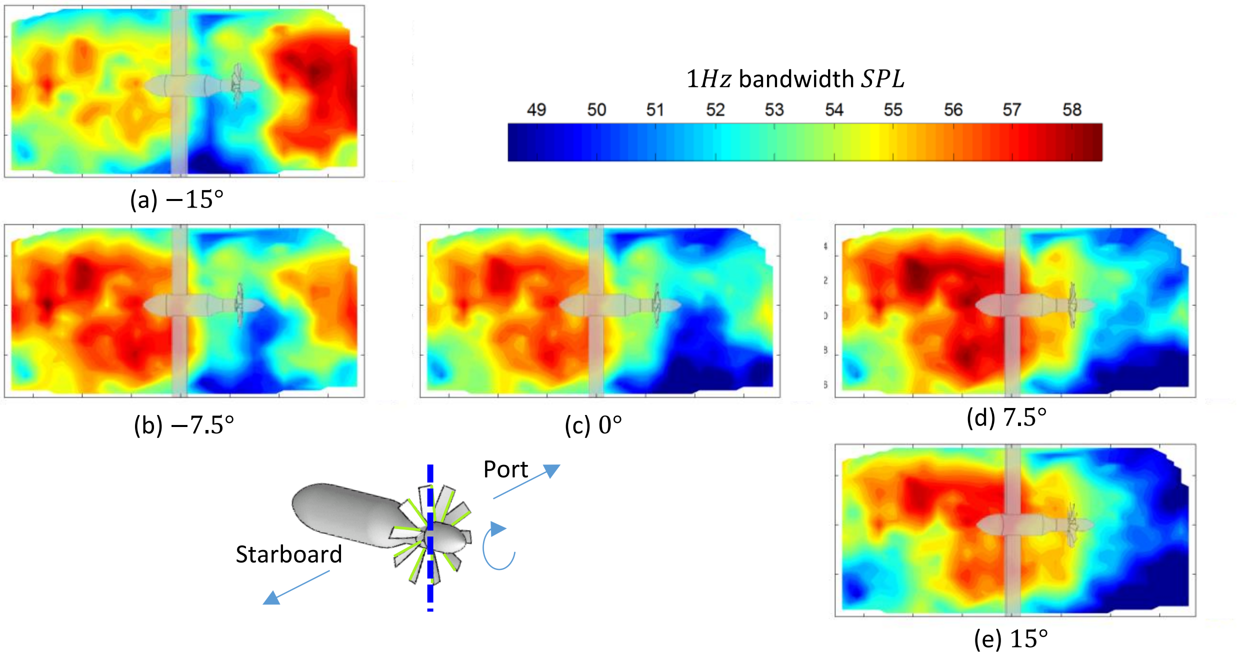

Figure 11. Contours of sound levels at 1BPF (547 Hz) measured on the starboard side of the rotor at an advance ratio J of 0.8 and center strike location in a plane at y =1.68-m using the phased array, as a function of rotor yaw angle. Divisions on vertical and horizontal axis are at intervals of 0.5 m.

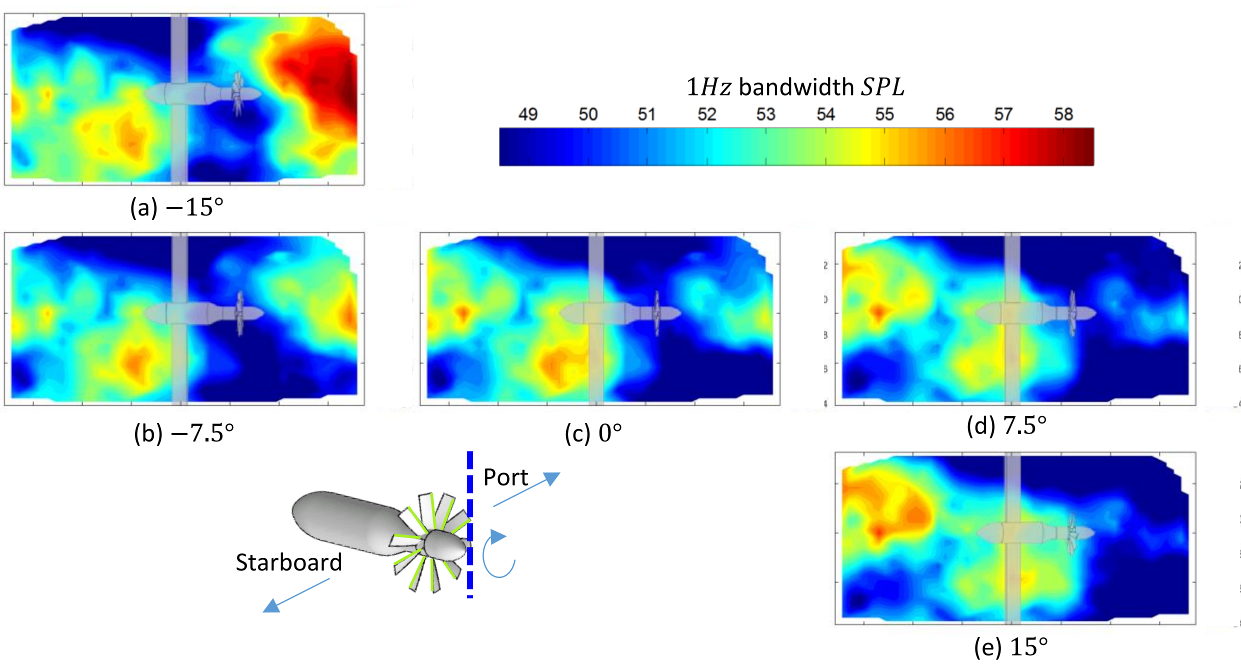

Figure 12. Contours of sound levels at 1BPF (547 Hz) measured on the starboard side of the rotor at an advance ratio J of 0.8 and 100% port strike location in a plane at y =1.68-m using the phased array, as a function of rotor yaw angle. Divisions on vertical and horizontal axis are at intervals of 0.5 m.

C. Turbulence measurements in the rotor frame

In order to predict the acoustic response of the rotor to the turbulent inflow, the distorted inflow itself must be known. The on-blade hotwire system was used to measure this directly, particularly the unsteady upwash which is the dominant component of the unsteady blade loading. The data were phase-averaged to compute mean and unsteady velocity components as a function of blade angle. The phase-averaging was completed by dividing the blade rotation into one degree bins. At the lowest rotational speed, this gives approximately 4250 samples per bin and a statistical sampling uncertainty of 2% in the phase-averaged values.

Figure 13 shows the mean-square unsteady upwash $\overline{u_p^2}$ profile through the wake as measured by the on-blade hotwire at 90% radius with the cylinder at the center strike position and U_∞ =10 m/s. The profiles measured during the top and bottom passes through the wake are plotted separately as contours as a function of advance ratio J. Note that profiles measured during the bottom pass appear shifted slightly (about $0.05R$) in y compared to those measured during the top pass, but are otherwise very similar. This is not distortion. It is because the blade orientation is reversed during the two passes and thus the orientation of the upwash component is different. Because of the anisotropy of the wake turbulence structure this results in a differently skewed profile. Distortion is apparent in the streamtube contraction that narrows the wake with increasing thrust and decreasing advance ratio. From J = 1.44 to 0.58, the width of the wake contracts by 16% before impact with the rotor face, but retains its roughly symmetric form. Note that peak upwash turbulence levels at low thrust (high J) are most similar to streamwise turbulence levels measured in the undisturbed wake (Figure 4(b)) when low-frequency flapping motions are filtered out.

Figure 14 again shows the unsteady upwash as seen by the probe at 90% radius, but in this case, the cylinder is at the 75% port strike location. Near zero-thrust, the center of the wake appears at the 75% R location as expected, but as the advance ratio decreases, the center of the wake is drawn across the rotor disk face towards its center, shifting by about 20% of the rotor radius at the lowest advance ratio. Comparing Figures 13 and 14, it appears that the streamtube contraction is more drastic when the center of the wake is on the edge of the rotor disk. This difference impacts both the wake turbulence and the produced noise. For this single probe position, the relative velocity of the probe increases with decreasing advance ratio. One may expect the far field noise from this particular blade strip of the rotor to increase roughly as the sixth power of velocity (dipole source efficiency), but the observed changes, both

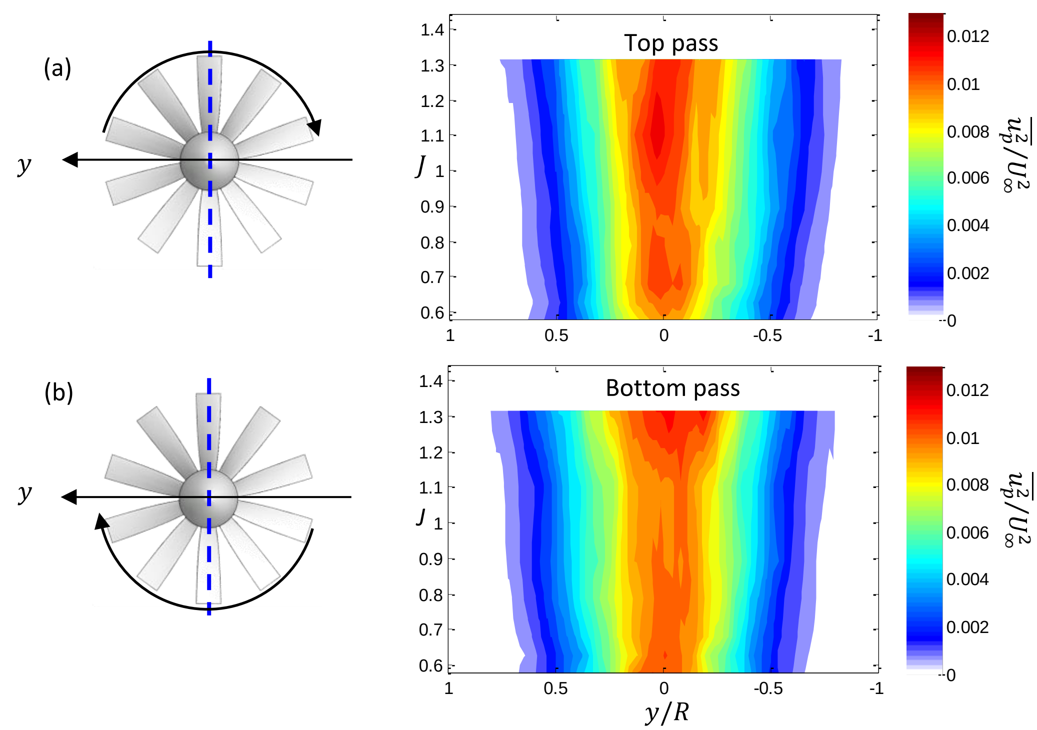

Figure 13. Profiles of mean square upwash velocity seen at the 90% rotor radius as a function of advance ratio with the wake striking the center of the rotor. Profiles measured (a) during the top (positive z) pass, and (b) during the bottom pass.

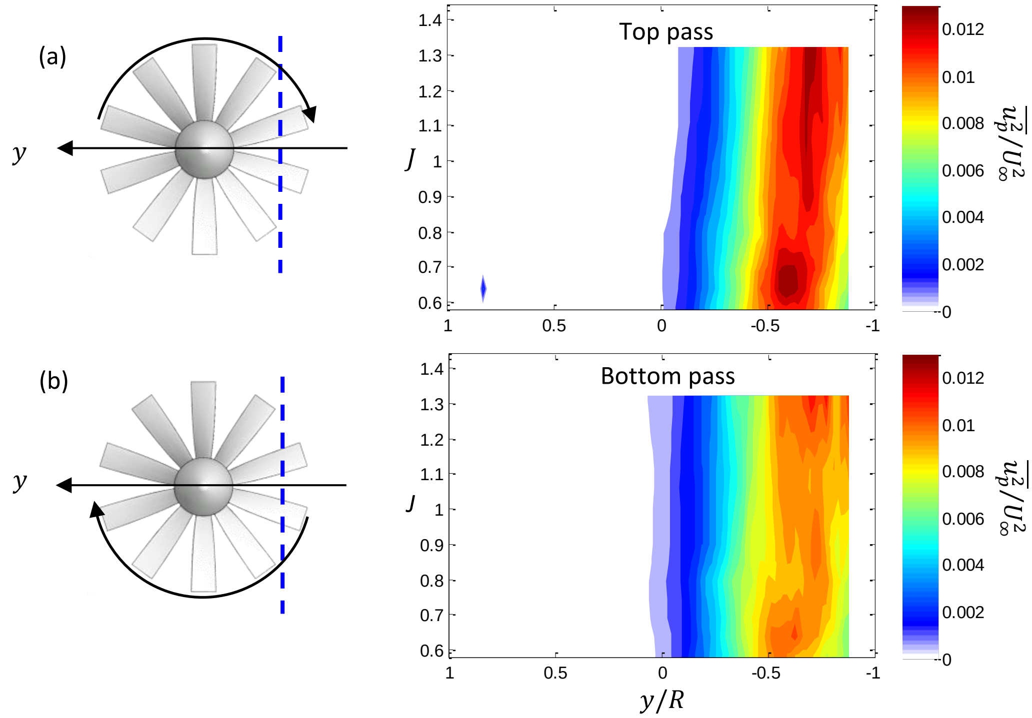

Figure 14. Profiles of mean square upwash velocity seen at the 90% rotor radius as a function of advance ratio with the wake striking at the 75% port location. Profiles measured (a) during the top (positive z) pass, and (b) during the bottom pass.

distortion and wake movement, must also be considered when predicting the noise at a particular observer location. The dipole for this particular section of blade has a rotating directivity pattern. Movement in the center of the wake slides the peak radiative efficiency for this particular strip to another observer location. Of course, this effect will get integrated across the entire rotor disk in a full strip theory approach. Accurate prediction of noise must fully account for this three-dimensional movement of the ingested wake even if the undisturbed wake could otherwise be considered two-dimensional and statistically stationary.

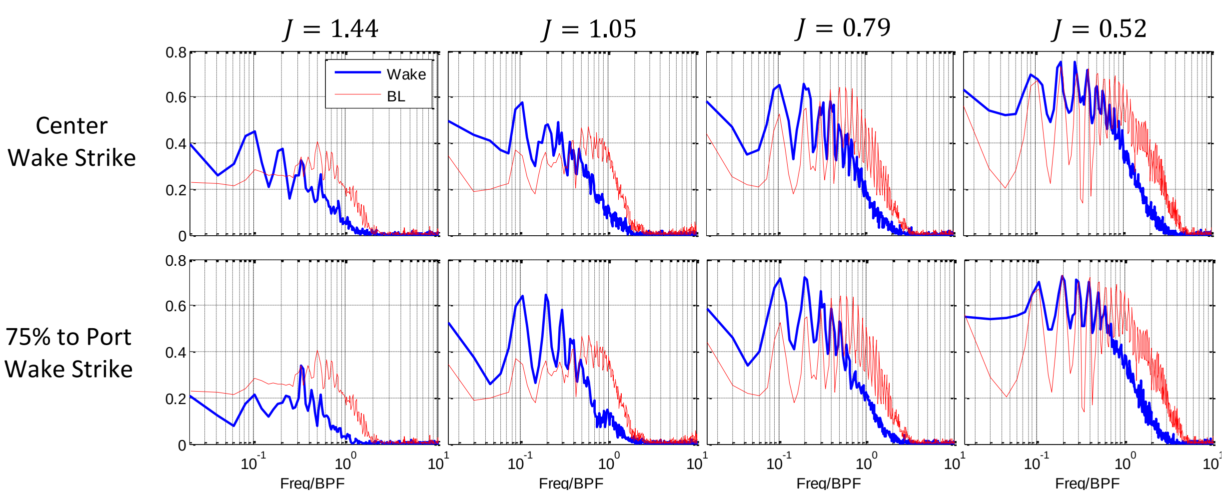

Figure 15. Coherence spectra between probes at 95% of the blade radius and 90% of the blade radius on a following blade at selected advance ratios for two strike locations. Spectra measured for boundary layer ingestion by Alexander *et al.* (2014) are included for comparison.

Coherence between the probe at 95%R on the leading blade and 90%R on the trailing blade are shown in Figure 15. These data are compared to the coherence measured by a similar probe combination measured for the turbulent boundary layer experiment [14] . Like in the boundary layer study, the broad coherence at lower frequencies, f/BPF<1, between the probe pair rises with decreasing advance ratio. This can be thought of as a straightforward effect of increase in rotor speed, decreasing the time between passes of the leading and trailing blade. Although, the coherence spectra from the cylinder wake tends to roll-off at lower non-dimensional frequency than the boundary layer study and has fewer sustained harmonics at the shaft rotation rate. These effects can be attributed to the release of the wall boundary condition. For the cylinder wake, the distortion and stretching of the approach turbulence is less severe than for the planar wall boundary layer. The wall itself increases the acceleration and streamwise extension of turbulence in the shear layer for any given operating condition. The coherence of the blades passing through this axially extended turbulence on multiple rotations produces the peaks at the shaft rate. At lower advance ratio, these near-wall turbulence structures are stretched and cut more times by a single blade then the structures in the cylinder wake.

IV. Conclusions

Measurements have been performed on a scaled version of a Sevik rotor ingesting a planar turbulent wake. The circular cylinder used to generate the wake was placed 20 cylinder diameters upstream of the rotor disk. Detailed measurements were made of the undisturbed wake, including three-component turbulence profiles and the full cross sectional 4-dimensional space time correlation function of its turbulence. Sound measurements were made of the wake ingestion into the rotor for a comprehensive range of rotor advance ratios varying from zero to high thrust, for rotor yaw angles out of the plane of the wake from -15 to 15 degrees, and for a range of wake strike positions on the rotor disk. Probes mounted on two of the rotor blades were used to measure upwash fluctuations seen in the rotating frame, as well as blade to blade coherence spectra. Comparisons have been made with flow and sound measurements made by Wisda *et al.* [12], Alexander *et al.* [14] and others during a previous studies of planar turbulent boundary layer ingestion into the same rotor.

The cylinder wake was found to produce an intense and anisotropic turbulent inflow with a width approximately equal to the rotor diameter. Streamwise correlations in the rotor were found to be dominated by vortex shedding at a Strouhal number of 0.19, the train of eddies producing correlated velocity fluctuations over time delays equivalent to the passage of about 6 rotor radii. Correlations in the spanwise direction extended over about 1 rotor radius. Sound spectra measured with the rotor showed haystacking at the blade passing frequency and higher harmonics for a range of thrusting conditions produced by multiple cutting of the same turbulent eddies by successive blades. Compared to boundary layer ingestion, wake ingestion produced much louder sound, because of the higher wake turbulence levels and the greater area of the rotor disk immersed. With the boundary layer, however, the haystacks are more distinct and extend to higher harmonics. This is partly because the boundary layer eddies have a much smaller spanwise extent so that successive blade interactions with the large eddies are more impulsive and partly because the stretching of boundary layer eddies entering the rotor is enhanced by the image of the rotor in the wall.

Yawing the rotor in the wake produces some change in the definition of the haystacks, due to the change in the correlation structure of the turbulence cut by the blades, but the major effect is a change in overall sound levels. This change is a directivity effect, the sound field being determined primarily by the observer angle relative to the rotor axis rather than the flow axis. Consistent with Alexander *et al.* [19] directivity is controlled by the compactness of the blade chord, but the non-compactness of the rotor as a whole. The sound has a dipole-like directivity in the direction of the blade normals where the rotor is cutting the most intense wake turbulence. This also controls the dependence of the sound field on wake strike location.

On-blade hot wire measurements reveal the distortion of the wake as it is drawn into the rotor. With the center of the wake striking the center of the rotor the principal effect of the distortion is the narrowing of the wake with increasing thrust due to streamline contraction. With the wake striking closer to the edge of the disk the principal effect is the drawing of the wake towards the center of the rotor disk increasing the area of turbulence interaction. Blade to blade coherence with the wake ingestion is greater at low frequencies than in the boundary layer because of the larger turbulence scales, but lower at high frequencies partly because of additional stretching produced by the wall boundary condition in the boundary layer flow.

Acknowledgements

The authors would first like to thank Henry Murray, Ian Clark and Anthony Millican for their assistance during the wind tunnel entries, and Mr. Michael Marcolini for his insightful observations and help with reviewing the manuscript. The authors would also like to thank the Office of Naval Research, in particular Dr. Ki-Han Kim, for their support of this research through grants N00014-14-1-0141 and N00014-16-1-2395.

References

[1] Sevik, M., Sound Radiation from Subsonic Rotor Subjected to Turbulence, in: International Symposium on Fluid Mechanics and Design of Turbomachinery, University Park, Pennsylvania, 1973.

[2] Scharpf, D.F., Mueller, T.J., An Experimental Investigation of the Sources of Propeller Noise due to the Ingestion of Turbulence at Low Speeds, Experiments in Fluids, 18 (1995) 277-287.

[3] Minniti, R.J.I., Blake, W.K., Mueller, T.J., Inferring Propeller Inflow and Radiation from Near-Field Response, Part 1: Analytic Development, AIAA Journal, 39 (2001) 1030-1036.

[4] Minniti, R.J.I., Blake, W.K., Mueller, T.J., Inferring Propeller Inflow and Radiation from Near-Field Response, Part 2: Empirical Application, AIAA Journal, 39 (2001) 1037-1046.

[5] Wojno, J.P., Mueller, T.J., Blake, W.K., Turbulence Ingestion Noise, Part 1: Experimental Characterization of Grid-Generated Turbulence, AIAA Journal, 40 (2002) 16-25.

[6] Wojno, J.P., Mueller, T.J., Blake, W.K., Turbulence Ingestion Noise, Part 2: Rotor Aeracoustic Response to Grid-Generated Turbulence, AIAA Journal, 40 (2002) 26-32.

[7] Ganz, U.W., Joppa, P.D., Patten, T.J., Scharpf, D.F., Boeing 18-Inch Fan Rig Broadband Noise Test, in, NASA, 1998.

[8] Stephens, D.B., Morris, S.C., Sound Generation by a Rotor Interacting with a Casing Turbulent Boundary Layer, AIAA Journal, 47 (2009) 2698-2708.

[9] Morton, M.A., Devenport, W.J., Glegg, S., Rotor Inflow Noise Caused by a Boundary Layer: Inflow Measurements and Noise Predictions, in: 18th AIAA/CEAS Aeroacoustics Conference, Colorado Springs, Colorado, 2012.

[10] Alexander, W.N., Devenport, W., Morton, M., Glegg, S., Noise from a Rotor Ingesting a Planar Turbulent Boundary Layer, in: 19th AIAA/CEAS Aeroacoustics Conference, Berlin, 2013.

[11] Wisda, D., Alexander, W.N., Devenport, W.J., Glegg, S.A., Boundary Layer Ingestion Noise and Turbulence Scale Analysis at High and Low Advance Ratios, in: 20th AIAA/CEAS Aeroacoustics Conference, Atlanta GA, 2014.

[12] Wisda, D., Murray, H., Alexander, N., Nelson, M.A., Devenport, W.J., Glegg, S., Flow Distortion and Noise Produced by a Thrusting Rotor Ingesting a Planar Turbulent Boundary Layer, in: Aviation 2015, Dallas, TX, 2015.

[13] Murray, H., Wisda, D., Alexander, N., Nelson, M.A., Devenport, W.J., Glegg, S., Sound and Distortion Produced by a Braking Rotor Operating in a Planar Boundary Layer with Application to Wind Turbines, in: Aviation 2015, Dallas, TX, 2015.

[14] Alexander, W.N., Devenport, W.J., Wisda, D., Morton, M.A., Glegg, S.A., Sound Radiated from a Rotor and Its Relation to Rotating Frame Measurements of Ingested Turbulence, in: 20th AIAA/CEAS Aeroacoustics Conference, Atlanta, GA, 2014.

[15] Glegg, S., Buono, A., Grant, J., Lachowski, F., Devenport, W., Alexander, N., Sound Radiation from a Rotor Partially Immersed in a Turbulent Boundary Layer, in: Aviation 2015, Dallas, TX, 2015.

[16] Glegg, S., Grant, J., Wisda, D., Murray, H., Alexander, N., Devenport, W., Broadband Noise from a Rotor at an Angle to the Mean Flow, in: AIAA Scitech 2016, San Deigo, CA, 2016.

[17] Murray, H.H., Turbulence and Sound Generated by a Rotor Operating Near a Wall, MS Thesis, Aerospace and Ocean Engineering, Virginia Tech, 2016.

[18] Glegg, S., Grant, J., Murray, H., Devenport, W., Alexander, N., Sound Radiation from a Rotor Operating at High Thrust Near a Wall, in: AIAA/CEAS 22nd Aeroacoustics Conference, Lyon, France, 2016.

[19] Alexander, W.N., Molinaro, N.J., Hickling, C., Murray, H., Devenport, W.J., Glegg, S.A., Phased Array Measurements of a Rotor Ingesting a Turbulent Shear Flow, in: 22nd AIAA/CEAS Aeroacoustics Conference, Lyon, France, 2016.

[20] Hickling, C., Alexander, N., Molinaro, N.J., Devenport, W., Glegg, S., Efficient Beamforming Techniques for Investigating Turbulence Ingestion Noise with an Inhomogeneous Inflow, in: 23rd AIAA/CEAS Aeroacoustics Conference, Denver, CO, 2017.

[21] Glegg, S., Grant, J., Alexander, N., Devenport, W., Sound Radiation from a Rotor Operating in the Wake of a Cylinder, in: AIAA SciTech, Grapevine, TX, 2017.

[22] Wang, J., Wang, K., Wang, M., Large-Eddy Simulation Study of Rotor Noise Generation in a Turbulent Wake, in: 23rd AIAA/CEAS Aeroacoustics Conference, Denver, CO, 2017.
[23] Devenport, W.J., Burdisso, R.A., Borgoltz, A., Ravetta, P.A., Barone, M.F., Brown, K.A., Morton, M.A., The Kevlar-walled anechoic wind tunnel, Journal of Sound and Vibration, 332 (2013) 3971-3991.
[24] Wittmer, K.S., Devenport, W.J., Zsoldos, J.S., A Four-Sensor Hot-Wire Probe System for Three-Component Velocity Measurements, Experiments in Fluids, 24 (1998) 416-423.
[25] Bearman, P.W., Corrections for the effect of ambient temperature drift on hot-wire measurements in incompressible flow, DISA Information, 11 (1971) 25-30.
[26] Molinaro, N.J., The Two Point Correlation Structure of a Cylinder Wake, MS Thesis, Aerospace and Ocean Engineering, Virginia Tech, 2017.
[27] Glegg, S.A.L., Devenport, W.J., Proper Orthogonal Decomposition of Turbulent Flows for Aeroacoustic and Hydroacoustic Applications, Journal of Sound and Vibration, 239 (2001) 767-784.
[28] Hersh, A.A., Soderman, P.T., Hayden, R.E., Investigation of Acoustic Effects of Leading-Edge Serrations on Airfoils, Journal of Aircraft, 11 (1974) 197-202.